How universal is the wetting aging in 2D materials

Xuan Chen[1†], Zhibin Yang[2†], Shizhe Feng[3†], Thaddeus Wayne Golbek[4], Wanghuai Xu[1], Hans-Jürgen Butt[5], Tobias Weidner[4], Zhiping Xu[3*], Jianhua Hao[2*], Zuankai Wang[1,6*]

[1]Department of Mechanical Engineering, City University of Hong Kong, Hong Kong 999077, China.

[2]Department of Applied Physics, The Hong Kong Polytechnic University, Hong Kong 999077, China.

[3]Applied Mechanics Laboratory, Department of Engineering Mechanics and Center for Nano and Micro Mechanics, Tsinghua University, Beijing 100084, China

[4]Department of Chemistry, Aarhus University, Aarhus 8000, Denmark.

[5]Max Planck Institut for Polymer Research, 55128 Mainz, Germany.

[6]Shenzhen Research Institute of City University of Hong Kong, Shenzhen 518057, China.

[†]These authors contribute equally to this work.

[*]Corresponding authors: jh.hao@polyu.edu.hk (J.H.), xuzp@tsinghua.edu.cn (Z.X.), zuanwang@cityu.edu.hk (Z.W.)

Abstract

Previous studies indicate that 2D materials such as graphene, WS_2 and MoS_2 deposited on oxidized silicon substrate are susceptible to aging due to the adsorption of airborne contamination. As a result, their surfaces become more hydrophobic. However, it is not clear how ubiquitous such a hydrophobisation is, and the interplay between the specific adsorbed species and resultant wetting aging remains elusive. Here, we report a pronounced and general hydrophilic-to-hydrophobic wetting aging on 2D InSe films, which is independent on the substrates to synthesize these films (silicon, glass, nickel, copper, aluminum oxide), though the extent of wetting aging is sensitive to the layer of films. Our findings are ascribed to the occurrence and enrichment of airborne contamination that contains alkyl chains. Our results also suggest that the wetting aging effect might be universal to a wide range of 2D materials.

Keywords: wetting aging effect, 2D materials, InSe, hydrophobisation, airborne contamination

Introduction

Since the discovery of graphene, two-dimensional (2D) materials such as transition metal dichalcogenides (TMDs), compounds from group IIIA (Ga, In) and the chalcogenide group VIA (S, Se and Te), have received explosive attention in fundamental understanding and applied implementation[1-6]. Underlying various multifunctional applications in e.g. nano-electrical devices, optoelectronics, and nanomedicine, in which 2D materials serve as either uniform coatings or fillers, lie a common need, an essential requirement to tune the interfacial properties of these materials to achieve superior performances. This is because, the behaviors and performances of these practical applications are closely dictated by the interfacial properties of 2D materials, individual or collective. Such a need becomes more heightened when considering the fact most of these applications are coupled with complex working conditions, which involves the flow of air and liquids, the fluctuation of temperature as well as pressure variations[7-12]. Thus, the understanding and controlling of the dynamic interaction of 2D materials with environments provides important insights that can potentially lead to a predictive framework for various applications.

Previous studies have shown that the partial wetting transparency of monolayer graphene can exert an influence on heat exchange between a graphene-supported copper substrate and water vapor[13, 14]. Recently, it was further demonstrated that the wettability of supported graphene and graphite is susceptible to airborne environment even though the surface is well protected[15, 16]. As an extension of graphene, WS_2 and MoS_2 materials have also been shown to exhibit the transition of wetting state as a result of the contamination by hydrocarbons adsorbed from ambient air[17-19]. Despite extensive progress, it remains difficult to identify and quantitatively measure the adsorbed species due to the rapid wetting transition in exposure to ambient conditions as well as the extremely thin nature of these 2D materials coatings. Moreover, previous studies on the aging effect of graphene, WS_2 and MoS_2 are mainly confined

on the oxidized silicon substrate, and thus it is not clear whether such an aging effect is general to different substrates.

In this work we seek to quantitatively probe how the wetting properties of 2D materials evolve under ambient environments. Of special interest is 2D layered InSe[20, 21], an emerging 2D layered semiconductor. As schematically shown in Fig. 1a, the InSe nanosheet is composed of stacked-layered Se-In-In-Se atomic structure interacted by van der van der Waals force. Its band gap can be tuned by the thickness between 1.26-2.20 eV, which offers potential applications such as ultrasensitive and broadband photodetection devices[22, 23]. We find that the pristine 2D layered InSe films are intrinsically hydrophilic, but exhibit pronounced hydrophilic-to-hydrophobic transition in response to air exposure at ambient conditions. We demonstrate that such an aging effect is also general to a wide range of substrates including silicon, glass, nickel, copper, aluminum oxide, which is due to the adsorptions of hydrocarbon compounds in air. Furthermore, we conduct molecular dynamic (MD) simulation to substantiate our conclusions.

Results

We applied a pulse laser deposition (PLD) process (Supplementary Fig. 1) to prepare InSe nanosheet[24, 25]. Briefly, the target of bulk InSe was first placed in front of the substrate with temperature maintained at 600℃. Then a KrF pulsed laser (λ = 248 nm) with 320 mJ energy and 10 Hz repetition rate was utilized to ablate the InSe target on the substrate in an ultra-high vacuum chamber. By careful control of the rotation of both target and substrates during the deposition process, uniform InSe nanosheets can be deposited over the entire substrate. In this work, we prepared mono- and few-layer InSe films on various substrates, including SiO_2/Si, glass, nickel, copper and aluminum oxide. The thickness of films can be precisely controlled by the number of laser pulses. Fig. 1b shows the optical image of the as-synthesized 1 nm thick (monolayer) InSe films coated on SiO_2/Si substrate, which display a large-area and continuous coverage. Fig. 1c presents the layered structure of the as-prepared InSe film on SiO_2/Si substrate as imaged by transmission electron microscopy (TEM). The film thickness is 10 nm,

corresponding to 10 layers. The diverse sequences of primitive layers in crystalline InSe bulk result in three different polytypes (β, γ, ε). To distinguish the phase of obtained films, we also performed Raman spectroscopy to characterize the structural fingerprint of various layered InSe nanosheets. Raman spectroscopy (Fig. 1d) showed A1′, A2″, E′ and E″ peaks, which are consistent with those reported before[22]. The spectra confirm the existence of a homogeneous films of ε-InSe. The intensity of the Raman peaks is significantly reduced with decreasing of film thickness, which is consistent with the suppressed van der Waals interactions in thinner film[26]. In addition, Raman mapping (Supplementary Fig. 2) demonstrates the good uniformity of the as-prepared InSe nanosheet over areas of at least 100 ×100 μm^2.

The water contact angle (WCA, θ_o) of the freshly prepared InSe monolayer deposited on SiO_2/Si substrates within 20 s of taking out of the PLD chamber is 54° (Fig. 2a). For statistics, 3~5 individual measurements were performed at different locations on each sample and the results were averaged to acquire the mean and standard deviation. WCA measurements were performed in ambient environments with a room temperature of 23°C and relative humidity of 50%. Note that the WCA of the bare SiO_2/Si substrate without the deposition of 2D materials is 36°. Thus, even a single InSe monolayer strongly influences wetting and screens the influence of the underlying SiO_2. It can be explained by the fact that InSe nanosheet is thick enough to effectively screen the interaction between water molecules and substrate material below the nanosheet[27]. The WCA rises to 62° within 10 mins, and eventually plateaus at 91°, reminiscence of a typical hydrophilic to hydrophobic transition. Further observations also show that the advancing CA follows a time-dependent augmentation, whereas the receding CA is relatively stable and varies between 20° and 40° (Supplementary Fig. 3). The contrast in the advancing and receding CAs implies that the structures of surface absorption may change when being wetted. Focusing on different monolayer 2D materials including InSe, WS_2[17], and MoS_2[18], we further compared the dynamic range of WCAs ($\triangle\theta$) after and previous to the air exposure in diverse time intervals. For effective comparison, all the 2D materials were deposited on SiO_2/Si substrate and three measurements under different exposure times were

conducted. As shown in Fig. 2b, under 24 hours' exposure, the $\triangle\theta$ of the InSe is 24°, which is much higher than those of WS_2, MoS_2, respectively.

Extending from monolayer TMDs materials, we continued to investigate the wetting properties for InSe films with increasing layers (4-layer, 10-layer, and bulk (20 nm)). For these freshly prepared InSe films, their WCAs were measured to vary between 50° and 65° (Supplementary Fig. 4). The variation of WCAs may be impacted by the roughness features generated by the PLD synthesis method. In contrast, after air exposure up to 24 hours, the WCAs increase monotonically with increasing layer (Fig. 2c), showing a marked layer-dependent wettability. As shown in Fig. 2c, their WCAs after aging increase to 100°-110°, which are also larger than that of the monolayer. The manifestation of layer-dependent wetting aging and enhancement on InSe multi-layer films suggests that the occurrence airborne contamination, which takes place both on the surface and the bulk. Given that the adsorption occurs on the surface alone, the WCAs after long period exposure should be indistinguishable. Thus, we hypothesize that the airborne contamination is the dominant factor, which will also create the formation of rough structures on the films.

Previous studies of wetting aging of TMDs materials have mainly focused on the oxidized silicon substrate[8, 17, 18]. Thus, it is unclear whether the wetting aging effect is also general to different substrates. Here, we tested InSe films coated on different substrates including glass, nickel, copper and aluminum oxide (inset of Fig. 2d). As shown in Fig. 2d, initially, the WCAs of all the fresh InSe samples deposited on various substrates vary from 35° to 55°, gradually increase when exposed to ambient conditions, and eventually reach values ranging from 100° to 115°. These measurements suggest that such the aging effect is general to different substrates.

To validate that the wetting aging effect is mediated by the adsorption of airborne contaminants, we further implemented thermal annealing on the aged 20 nm InSe film on SiO_2/Si substrates to fully remove adsorbed contaminations. Previously, it has been demonstrated that thermal annealing can effectively remove the contaminants adsorbed on 2D materials such as graphene and WS_2[15, 17]. The sample was first annealed in a furnace at 350ºC for 2 hours and then cooled down to ambient temperature under argon atmosphere to prevent

oxidation. The WCA of the freshly treated sample was 57°, which is consistent with that of the pristine surface and much smaller than that of the aged sample (Fig. 3a). Then, there is a monotonic increase in WCA until reaching the saturated value of 100°. Again, the value is consistent with the aging phenomenon discussed above. Thus, the reversible switching of the WCAs in response to annealing demonstrates that the aging effect is indeed caused by the adsorption of airborne contaminants.

To identify the specific adsorbed contaminants, we conducted time-dependent Fourier-transform infrared spectroscopy (FTIR) measurement of aged 20 nm InSe film on SiO_2/Si substrate (Fig. 3b). Two peaks emerged at 2,850 cm^{-1} and 2,930 cm^{-1}. They are assigned to two vibrations of methylene group $(-(CH_2)_n-)$[28]. We attribute them to an adsorbed alkyl-containing contaminant. These two methylene peaks disappear (Supplementary Fig. 5) when the aged sample is annealed under argon atmosphere; in this case the FTIR measurement was conducted right after removing the samples out of the furnace (within five mins). Thus, the amount of adsorbed contaminants is still insignificant. When exposing the samples for more than an hour to air, the methylene peaks re-emerge as a result of re-adsorption of contaminants. Thus, we propose that the aging effect of 2D InSe is caused by a continuous accumulation of hydrocarbons. However, dislike the relatively sharp change in the WCA measurement, the gradual and subtle adsorption of hydrocarbon absorption on the aged sample could not be determined in the spectrum due to the limitation of the experimental resolution.

We further carried out X-ray photoelectron spectroscopy (XPS) measurements[29, 30, 31] on the 20 nm 2D InSe film to reveal the chemical specificity of the adsorbed contaminants. As shown in Fig. 4a, the XPS spectra show the presence of a C_{1s} peak, an important element responsible for the wetting aging effect. To quantitatively measure the amount of adsorbed carbon, we treated the aged InSe film under an Ar_{500+} ion beam (5 keV) for 60 seconds to completely remove the adsorbed contaminants from the surface. As displayed in Fig. 4b, there is a 5.6% reduction in the measured atomic percent of carbon for the clean sample whereas the atomic percent of In and Se significantly increase by 13.9% and 6.5%, respectively (details can be found in Supplementary Table 1). We also compared the high-resolution spectra for the aged

samples with and without treatment. As shown in Fig. 4c, for the aged sample, the representative spectra peaks at 285.0 eV, 286.5 eV, and 289.0 eV are assigned to the C-C, C-O and the oxidized carbon, respectively. These important results, otherwise impossible to be derived from FTIR, clearly reveal the chemical states of the aged InSe film. In contrast, the high-resolution spectra obtained from the clean sample indicate that the carbon peaks vanish and only the Se auger peak (from the Al Kα X-ray source) remains (Fig. 4c)[32]. Similar trend is also manifested on InSe surface of 4 nm thick (Supplementary Fig. 6-8).

To identify the effect of adsorbed contaminants on surface wettability, we carried out MD simulation to predict how the WCAs of monolayer InSe vary with the coverage of hydrocarbon chains. The model is built on the deposition of a quasi-2D droplet on the substrate, which is composed of monolayer InSe as well as n-alkane chains (representative long $C_{50}H_{102}$ chains or short $C_{20}H_{42}$ chains) distributed orderly on the InSe surface (Fig. 5a). The interaction between InSe and oxygen atoms in the water molecules is described by the 12-6 Lennard-Jones potential function, in which the corresponding parameters are determined from the measured WCAs on the intact InSe surface. Other forcefield parameters are introduced in the method section. By fitting the converged density contours of the water droplet, the theoretical WCAs can be accordingly calculated from the simulations[33]. As shown in Fig. 5b, the predicted WCAs are linearly proportional to the areal coverage of n-alkanes, validating that the wetting transition observed on 2D InSe surface is indeed dictated by the gradual adsorption of airborne hydrocarbons.

The enhanced hydrophobicity as a result of surface adsorption of hydrocarbon containing alkyl segments on hydrophilic nanosheets such as InSe, WS_2 and MoS_2 can be captured in the Wenzel model[34, 35]. Briefly, the WCA(θ) can be expressed as a weighted average of the WCA of each component of the surface, *e.g.* intact InSe or contaminants, expressed as

$$\cos\theta = (1-c)\cos\theta_o + cr\cos\theta_c$$

where c is the coverage fraction of contaminants, θ_c is the effective contact angle of the contaminated area. $r = (w+2h)/w$ is the roughness owing to the introduction of *n*-alkenes, defined as the ratio of the surface area of alkene chains to its projected area, where w = 0.2 nm,

h = 0.7 nm are the width and depth of the *n*-alkenes measured from the MD models. By fitting the WCAs simulated at given θ_c = ~110° for $C_{20}H_{42}$ or $C_{50}H_{102}$, the relationship between c and θ can be obtained, *i.e.*, c=0.301(0.588-cosθ). Thus, for a specific measured value of θ, the corresponding concentration of hydrocarbon adsorption can be extracted (fitted data in Fig. 5b). For example, after 24 h exposure to air, the WCA of a InSe monolayer is stabilized at 90°, corresponding to a theoretically predicted areal coverage c ~ 17%. Note that for the multi-layer nanosheets, the real areal coverage should be slightly higher due to its nature of adsorption. Although such theoretical data could not be validated by experimental measurements, our simple model still quantitatively explains the universal wetting aging behaviors of the 2D materials under ambient conditions as we studied in experiments.

Conclusion

We report a pronounced time-dependent, hydrophilic-to-hydrophobic wetting aging manifested on 2D InSe films under ambient conditions. In particular, we discover that the wetting aging is layer-dependent, which is attributed to the adsorption of hydrocarbons containing alkyl segments from the surrounding air. This hypothesis is based on XPS measurements, which indicate the occurrence and enrichment of carbon on the surface, and FTIR results, which indicate the presence of methylene groups. We also reveal how the adsorption and enrichment of the alkyl segments results in enhanced hydrophobisation. Moreover, our study suggests that the hydrophilic-to-hydrophobic wetting transition is general to 2D materials, regardless of the substrates used to synthesize these materials.

Methods

Synthesis The ultrathin 2D InSe films were prepared on various substrates, including SiO_2 (300 nm)/Si, glass, nickel, copper and aluminum oxide by PLD. The target of bulk InSe was placed ≈ 4cm in front of the substrate. The chamber was evacuated to a pressure of 1.5×10^{-7} Torr. The substrate temperature was maintained at 600℃ by using an integrated thermocouple. An energetic UV pulsed laser was utilized to strike the surface of InSe target, which vaporize

a large number of atoms, molecules and clusters, and then condensing to the film on the preheated substrate. During deposition, the chamber pressure, substrate temperature and laser beam power were precisely controlled to acquire the high-quality film. The InSe nanosheet covered the entire substrate uniformly in the sake of rotation of both target and substrates during the deposition process. As soon as deposition being finished, the as-grown nanosheet was cooled down to room temperature. The polycrystalline feature of the film was confirmed by XRD and TEM results, respectively. The thickness of the film was measured by cross-sectional TEM (JEOL JIB-4500), which is applied by FIB (JEOL JIB-4500) milling. The as-prepared films were then transferred onto a copper grid for TEM characterization. Raman spectra was obtained by a high-resolution confocal μ-Raman system (Horiba, HR 800) equipped with 488 nm laser source.

Water contact angle measurement The WCA experiment was performed using a Kruss DSA 100 WCA instrument for images capture. The tangent drop shape analysis method was used to determine the contact angles. Advancing and receding angles measurement was recorded by a CCD camera through adding or withdrawing deionized water to and from a sessile drop.

FTIR characterization FTIR spectra were collected with a Bruker Tensor 27 FTIR Spectrometer in absorbance mode using DigiTect^{TM}detector (4000-600 cm^{-1} spectral range). Before measurements, a background spectrum was collected without having the crystal contacting the sample. Each sample spectrum was collected for 16 scans with a resolution of 4 cm^{-1} and a total acquisition time of 1 min. After collecting each spectrum, the crystal was detached from the surface to allow surface aging.

XPS measurement XPS experiments were performed on a Kratos AXIS Ultra DLD instrument equipped with a monochromatic Al Kα X-ray source (hν = 1486.6 eV). All spectra were collected in hybrid mode at a take-off angle of 55° (angle between the sample surface plane and the axis of the analyzer lens). The spectra were collected at fresh spots on the sample (n=3)

and were charge corrected to the C_{1s} aliphatic carbon binding energy at 285.0 eV and a linear background was subtracted for all peak area quantifications. Analyzer pass energy of 80 eV was used for compositional survey scans of C_{1s}, O_{1s}, Se_{3d}, and In_{3d}. High-resolution scans of C_{1s}, Se_{3d}, and In_{3d} elements were collected at an analyzer pass energy of 20 eV. Compositions and fits of the high-resolution scans were produced in CasaXPS. A depth profile was done with 1 cycle and XPS spectrum was collected after exposing the surface to the cluster for 60 seconds. For sputtering, a gas cluster source using an Ar500+ gas cluster ion beam with a kinetic energy of 5 keV.

MD simulation We perform molecular dynamics simulations using the large-scale atomic/molecular massively parallel simulator (LAMMPS)[36]. The all-atom optimized potentials for liquid simulations (OPLS-AA) are used for InSe[37], and the extended simple-point-charge model (SPC/E) for water molecules, which is widely adopted for MD simulations of water and WCA calculation[38, 39]. The interactions between InSe monolayers and oxygen atoms in the water molecules is described using the 12-6 L-J potential functions, with parameters $\varepsilon_{\text{In-O}}$ = 0.0090 eV, $\sigma_{\text{In-O}}$ = 0.327 nm, $\varepsilon_{\text{Se-O}}$ = 0.0110 eV, $\sigma_{\text{Se-O}}$ = 0.317 nm, and the cut-off is made at 1.2 nm. These parameters are determined by fitting experimentally-measured WCAs for clean InSe monolayers. The L-J potential parameters used for *n*-alkanes are $\varepsilon_{\text{C-O}}$ = 0.0084 eV, $\sigma_{\text{C-O}}$ = 0.336 nm. The long-range Coulomb interactions are computed by the particle-particle particle-mesh algorithm (PPPM)[40]. The time step chosen for the equation-of-motion integration is 1 fs, with the SHAKE algorithm applied for the stretching terms between oxygen and hydrogen atoms of water to reduce high-frequency vibrations that require a very short time step.

A quasi-2D droplet model is used here to predict the water contact angle (WCA) of the InSe surfaces with and without hydrocarbon contamination[27]. A half-cylindrical droplet with diameter of 2 nm (8500 water molecules) is placed on an InSe slab (70 nm× 3 nm, with/without alkane-chain coverage). Periodic boundary conditions (PBCs) are enforced in the in-plane directions, while an open boundary is set up in the out-of-plane direction. We carried out

simulations with both long $C_{50}H_{102}$ chains and short $C_{20}H_{42}$ chains, which are chosen as representative hydrophobic, hydrocarbon chains. The alkyl chains are placed in parallel on the substrate in a centered rectangular lattice. Different lattice constants were used to tune the areal coverage.

Lattice dynamics of the polymer-coated InSe substrate is constrained, and the *n*-alkanes distributed at the solid-liquid interface formed as a flat monolayer (Fig. 5a)[41, 42]. The water molecules are equilibrated in an NVT ensemble using a Berendsen thermostat at 300 K. WCA is measured by fitting a water isochore extracted from the time-averaged water density map over 3 ns, through a dense spatial mesh with a grid spacing of 0.05 nm[43]. Here the liquid-vapor interface is defined as the contour line with a density level at half of the bulk value. The Werder method[44] is used then to fit the cross-section profile of the interface into an arc, where the WCA is calculated as the contingence angle at the basal plane, that is, the surface of hydrocarbon layers (~ 0.5 nm above InSe).

References

1. Lei, S.; Wang, X.; Li, B.; Kang, J.; He, Y.; George, A.; Ge, L.; Gong, Y.; Dong, P.; Jin, Z.; Brunetto, G.; Chen, W.; Lin, Z. T.; Baines, R.; Galvao, D. S.; Lou, J.; Barrera, E.; Banerjee, K.; Vajtai, R.; Ajayan, P., Surface functionalization of two-dimensional metal chalcogenides by Lewis acid-base chemistry. *Nat. Nanotechnol.* **2016,** *11* (5), 465-71.
2. Chhowalla, M.; Shin, H. S.; Eda, G.; Li, L. J.; Loh, K. P.; Zhang, H., The chemistry of two-dimensional layered transition metal dichalcogenide nanosheets. *Nat. Chem.* **2013,** *5* (4), 263-75.
3. Lopez-Sanchez, O.; Lembke, D.; Kayci, M.; Radenovic, A.; Kis, A., Ultrasensitive photodetectors based on monolayer MoS_2. *Nat. Nanotechnol.* **2013,** *8* (7), 497-501.
4. Jung, Y.; Zhou, Y.; Cha, J. J., Intercalation in two-dimensional transition metal chalcogenides. *Inorg. Chem. Front.* **2016,** *3* (4), 452-463.
5. Eksik, O.; Gao, J.; Shojaee, S. A.; Thomas, A.; Chow, P.; Bartolucci, S. F.; Lucca, D. A.; Koratkar, N., Epoxy nanocomposites with two-dimensional transition metal dichalcogenide additives. *ACS Nano* **2014,** *8* (5), 5282-9.
6. Huang, W.; Gan, L.; Li, H.; Ma, Y.; Zhai, T., 2D layered group IIIA metal chalcogenides: synthesis, properties and applications in electronics and optoelectronics. *CrystEngComm* **2016,** *18* (22), 3968-3984.
7. Radisavljevic, B.; Radenovic, A.; Brivio, J.; Giacometti, V.; Kis, A., Single-layer MoS_2 transistors. *Nat. Nanotechnol.* **2011,** *6* (3), 147-50.
8. Gaur, A. P.; Sahoo, S.; Ahmadi, M.; Dash, S. P.; Guinel, M. J.; Katiyar, R. S., Surface energy engineering for tunable wettability through controlled synthesis of MoS_2. *Nano Lett* **2014,** *14* (8), 4314-21.
9. Franklin, A. D., Nanomaterials in transistors: From high-performance to thin-film applications. *Science* **2015,** *349* (6249), aab2750.
10. Fiori, G.; Bonaccorso, F.; Iannaccone, G.; Palacios, T.; Neumaier, D.; Seabaugh, A.; Banerjee, S. K.; Colombo, L., Electronics based on two-dimensional materials. *Nat. Nanotechnol.* **2014,** *9* (10), 768-79.
11. Britnell, L.; Ribeiro, R. M.; Eckmann, A.; Jalil, R.; Belle, B. D.; Mishchenko, A.; Kim, Y. J.; Gorbachev, R. V.; Georgiou, T.; Morozov, S. V.; Grigorenko, A. N.; Geim, A. K.; Casiraghi, C.; Castro Neto, A. H.; Novoselov, K. S., Strong light-matter interactions in heterostructures of atomically thin films. *Science* **2013,** *340* (6138), 1311-4.
12. Zhao, M.; Ye, Y.; Han, Y.; Xia, Y.; Zhu, H.; Wang, S.; Wang, Y.; Muller, D. A.; Zhang, X., Large-scale chemical assembly of atomically thin transistors and circuits. *Nat. Nanotechnol.* **2016,** *11* (11), 954-959.
13. Rafiee, J.; Mi, X.; Gullapalli, H.; Thomas, A. V.; Yavari, F.; Shi, Y.; Ajayan, P. M.; Koratkar, N. A., Wetting transparency of graphene. *Nat. Mater.* **2012,** *11* (3), 217-22.
14. Kim, G.T.; Gim, S.J.; Cho, S.M.; Koratkar, N.; Oh, I.-K., Wetting-transparent graphene films for hydrophobic water-harvesting surfaces. *Adv. Mater.* **2014,** *26* (30), 5166-5172.
15. Li, Z.; Wang, Y.; Kozbial, A.; Shenoy, G.; Zhou, F.; McGinley, R.; Ireland, P.; Morganstein, B.; Kunkel, A.; Surwade, S. P.; Li, L.; Liu, H., Effect of airborne contaminants on the wettability of supported graphene and graphite. *Nat. Mater.* **2013,** *12* (10), 925-31.

16. Aria, A. I.; Kidambi, P. R.; Weatherup, R. S.; Xiao, L.; Williams, J. A.; Hofmann, S., Time evolution of the wettability of supported graphene under ambient air exposure. *J. Phys. Chem. C* **2016,** *120* (4), 2215-2224.
17. Chow, P. K.; Singh, E.; Viana, B. C.; Gao, J.; Luo, J.; Li, J.; Lin, Z.; Elias, A. L.; Shi, Y.; Wang, Z.; Terrones, M.; Koratkar, N., Wetting of mono and few-layered WS_2 and MoS_2 films supported on Si/SiO_2 substrates. *ACS Nano* **2015,** *9* (3), 3023-31.
18. Kozbial, A.; Gong, X.; Liu, H.; Li, L., Understanding the intrinsic water wettability of molybdenum disulfide (MoS_2). *Langmuir* **2015,** *31* (30), 8429-35.
19. Zhou, Y.; Reed, E. J., Microscopic origins of the variability of water contact angle with adsorbed contaminants on layered materials. *J. Phys. Chem. C* **2018,** *122* (32), 18520-18527.
20. Camara, M. O. D.; Mauger, A.; Devos, I., Electronic structure of the layer compounds GaSe and InSe in a tight-binding approach. *Phys. Rev. B* **2002,** *65* (12).
21. Bandurin, D. A.; Tyurnina, A. V.; Yu, G. L.; Mishchenko, A.; Zolyomi, V.; Morozov, S. V.; Kumar, R. K.; Gorbachev, R. V.; Kudrynskyi, Z. R.; Pezzini, S.; Kovalyuk, Z. D.; Zeitler, U.; Novoselov, K. S.; Patane, A.; Eaves, L.; Grigorieva, I. V.; Fal'ko, V. I.; Geim, A. K.; Cao, Y., High electron mobility, quantum Hall effect and anomalous optical response in atomically thin InSe. *Nat. Nanotechnol.* **2017,** *12* (3), 223-227.
22. Tamalampudi, S. R.; Lu, Y. Y.; Kumar, U. R.; Sankar, R.; Liao, C. D.; Moorthy, B. K.; Cheng, C. H.; Chou, F. C.; Chen, Y. T., High performance and bendable few-layered InSe photodetectors with broad spectral response. *Nano Lett* **2014,** *14* (5), 2800-6.
23. Yang, Z.; Jie, W.; Mak, C. H.; Lin, S.; Lin, H.; Yang, X.; Yan, F.; Lau, S. P.; Hao, J., Wafer-scale synthesis of high-quality semiconducting two-dimensional layered InSe with broadband photoresponse. *ACS Nano* **2017,** *11* (4), 4225-4236.
24. Hao, J.; Zhang, Y.; Wei, X., Electric-induced enhancement and modulation of upconversion photoluminescence in epitaxial $BaTiO_3$:Yb/Er thin films. *Angew. Chem. Int. Ed. Engl.* **2011,** *50* (30), 6876-80.
25. Zhang, Y.; Gao, G.; Chan, H. L.; Dai, J.; Wang, Y.; Hao, J., Piezo-phototronic effect-induced dual-mode light and ultrasound emissions from ZnS:Mn/PMN-PT thin-film structures. *Adv. Mater.* **2012,** *24* (13), 1729-35.
26. Yan, M.; Wang, E.; Zhou, X.; Zhang, G.; Zhang, H.; Zhang, K.; Yao, W.; Lu, N.; Yang, S.; Wu, S., High quality atomically thin $PtSe_2$ films grown by molecular beam epitaxy. *2D Mater.* **2017,** *4* (4), 045015.
27. Gurarslan, A.; Jiao, S.; Li, T. D.; Li, G.; Yu, Y.; Gao, Y.; Riedo, E.; Xu, Z.; Cao, L., Van der waals force isolation of monolayer MoS_2. *Adv. Mater.* **2016,** *28* (45), 10055-10060.
28. Shinozaki, A.; Arima, K.; Morita, M.; Kojima, I.; Azuma, Y., FTIR-ATR evaluation of organic contaminant cleaning methods for SiO_2 surfaces. *Anal. Sci.* **2003,** *19* (11), 1557-9.
29. Weidner, T.; Breen, N. F.; Drobny, G. P.; Castner, D. G., Amide or amine: determining the origin of the 3300 cm^{-1} NH mode in protein SFG spectra using 15N isotope labels. *J. Phys. Chem. B* **2009,** *113* (47), 15423-15426.
30. Techane, S. D.; Gamble, L. J.; Castner, D. G., Multi-technique characterization of self-

assembled carboxylic acid terminated alkanethiol monolayers on nanoparticle and flat gold surfaces. *J. Phys. Chem. C* **2011,** *115* (19), 9432-9441.

31. Zorn, G.; Dave, S. R.; Weidner, T.; Gao, X.; Castner, D. G., Direct characterization of polymer encapsulated CdSe/CdS/ZnS quantum dots. *Surf. Sci.* **2016,** *648*, 339-344.
32. Moulder, J. F. J. C., Handbook of x-ray photoelectron spectroscopy: A reference book of standard spectra for identification and interpretation of XPS data. *Perkin-Elmer Corporation* **1992**.
33. Wei, N.; Lv, C.; Xu, Z., Wetting of graphene oxide: A molecular dynamics study. *Langmuir* **2014,** *30* (12), 3572-3578.
34. Wenzel, R. N., Resistance of solid surfaces to wetting by water. *Ind. Eng. Chem.* **1936,** *28* (8), 988-994.
35. Zheng, Q.S.; Yu, Y.; Zhao, Z.H., Effects of hydraulic pressure on the stability and transition of wetting modes of superhydrophobic surfaces. *Langmuir* **2005,** *21* (26), 12207-12212.
36. Plimpton, S., Fast parallel algorithms for short-range molecular-dynamics. *J. Comput. Phys.* **1995,** *117* (1), 1-19.
37. Chen, C.; Ma, M.; Jin, K.; Liu, J. Z.; Shen, L.; Zheng, Q.; Xu, Z., Nanoscale fluid-structure interaction: flow resistance and energy transfer between water and carbon nanotubes. *Phys. Rev. E Stat. Nonlin. Soft Matter Phys.* **2011,** *84* (4 Pt 2), 046314.
38. Zhu, S. B.; Fillingim, T. G.; Robinson, G. W., Flexible simple point-charge water in a self-supporting thin-film. *J. Phys. Chem.***1991,** *95* (2), 1002-1006.
39. Dančová, P.; Vinš, V.; Celný, D.; Planková, B.; Němec, T.; Duška, M.; Hrubý, J.; Veselý, M., Molecular simulations of the vapor-liquid phase interfaces of pure water modeled with the SPC/E and the TIP4P/2005 molecular models. *EPJ Web of Conferences* **2016,** *114*.
40. Hockney, R.; Eastwood, J., Computer simulation using particles Taylor & Francis. Inc: 1988.
41. Xia, T. K.; Ouyang, J.; Ribarsky, M. W.; Landman, U., Interfacial alkane films. *Phys. Rev. Lett* **1992,** *69* (13), 1967-1970.
42. Balasubramanian, S.; Klein, M. L.; Siepmann, J. I., Simulation studies of ultrathin films of linear and branched alkanes on a metal substrate. *J. Phys. Chem.* **1996,** *100* (29), 11960-11963.
43. Wei, N.; Lv, C.; Xu, Z., Wetting of graphene oxide: a molecular dynamics study. *Langmuir* **2014,** *30* (12), 3572-8.
44. Werder, T.; Walther, J. H.; Jaffe, R. L.; Halicioglu, T.; Koumoutsakos, P., On the water-carbon interaction for use in molecular dynamics simulations of graphite and carbon nanotubes. *J. Phys. Chem. B* **2008,** *112* (44), 14090-14090.

Acknowledge

We acknowledge the financial support from Research Grants Council of Hong Kong (No.11217518, No. C1018-17G, No. 11275216, No. 11218417), City University of Hong Kong (No. 9680212, No. 9610375), Shenzhen Science and Technology Innovation Council (No. JCYJ20170413141208098), The Hong Kong Polytechnic University (RGC GRF No. PolyU 153023/18P).

Author Contributions

Z.W. and J.H. supervised the research. X.C., Z.Y., S.F. and W.X. designed the experiment. Z.B. synthesized the samples. T.G., H.B., and X.C. conducted the characterizations. X.C. and S.F. analyzed the data. S.F. and Z.X. performed the simulation. X.C., Z.W., Z.Y., J.H., S.F., and Z.X. wrote the paper and all the authors discussed the manuscript.

Competing interests

The authors declare no competing interests.

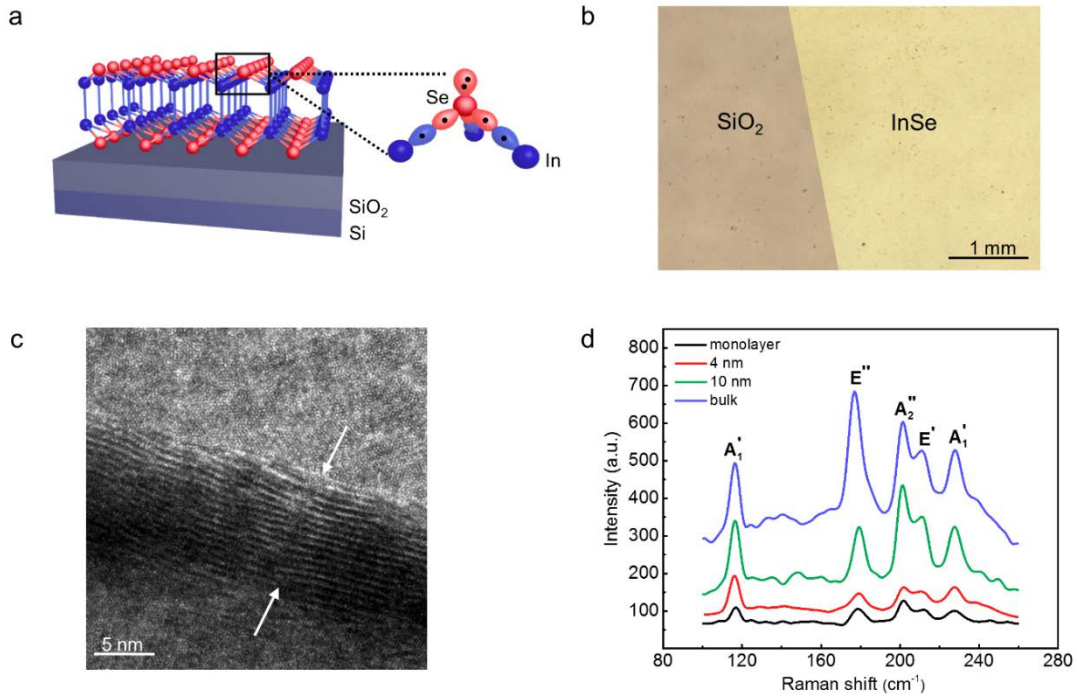

Figure 1 | InSe film deposition. (a) Schematic of monolayer InSe film on an oxidized silicon substrate. The thickness of SiO_2 is 300 nm. **(b)** Optical micrograph of 1 nm thick InSe on an oxidized silicon substrate. **(c)** Cross section TEM image of 10 nm InSe film. **(d)** Raman spectra of InSe films of different thickness, all of which are deposited on SiO_2/Si substrates. Here, monolayer (black), 4 nm (red),10nm (green) and bulk (20 nm, blue).

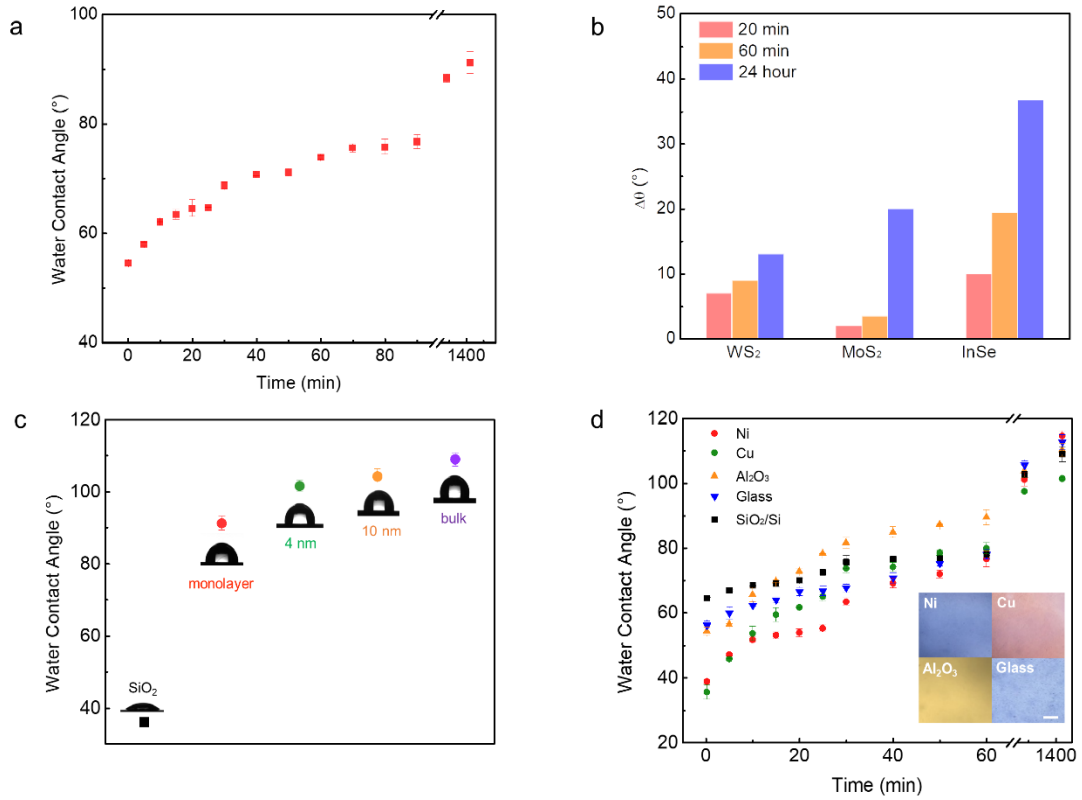

Figure 2 | Wetting aging dynamics of 2D materials. (a) Water contact angle (WCA) monolayer InSe film on Si/SiO_2 substrate. **(b)** Dynamic variation of WCA on monolayer InSe, WS_2 and MoS_2 after air exposure of 20 mins, 60 mins and 24 hours, respectively. **(c)** WCA measurement for InSe film with varying layers after air exposure up to 24 hours. **(d)** WCA measurement of bulk InSe films synthesized on different substrates. The insect shows optical micrograph of large-area continuous films coated on the corresponding substrates (scale bar is 200 nm).

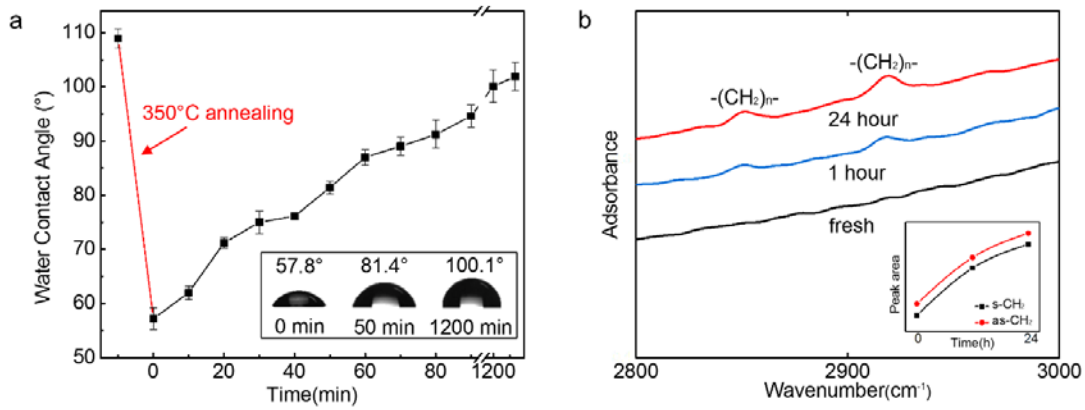

Figure 3 | Revealing the effect of contaminants on wettability and characterizing the components of airborne contaminants. (a) WCA measurement of a 20 nm InSe film on SiO_2/Si substrate over time after 350℃ thermal annealing. Sample was taken out of CVD chamber at time 0. **(b)** FTIR-ATR spectra for InSe film as a function of time after air exposure. The spectra reveal a rising volume of organic species $–(CH_2)_n–$ (2,850 cm^{-1} & 2,930 cm^{-1}).

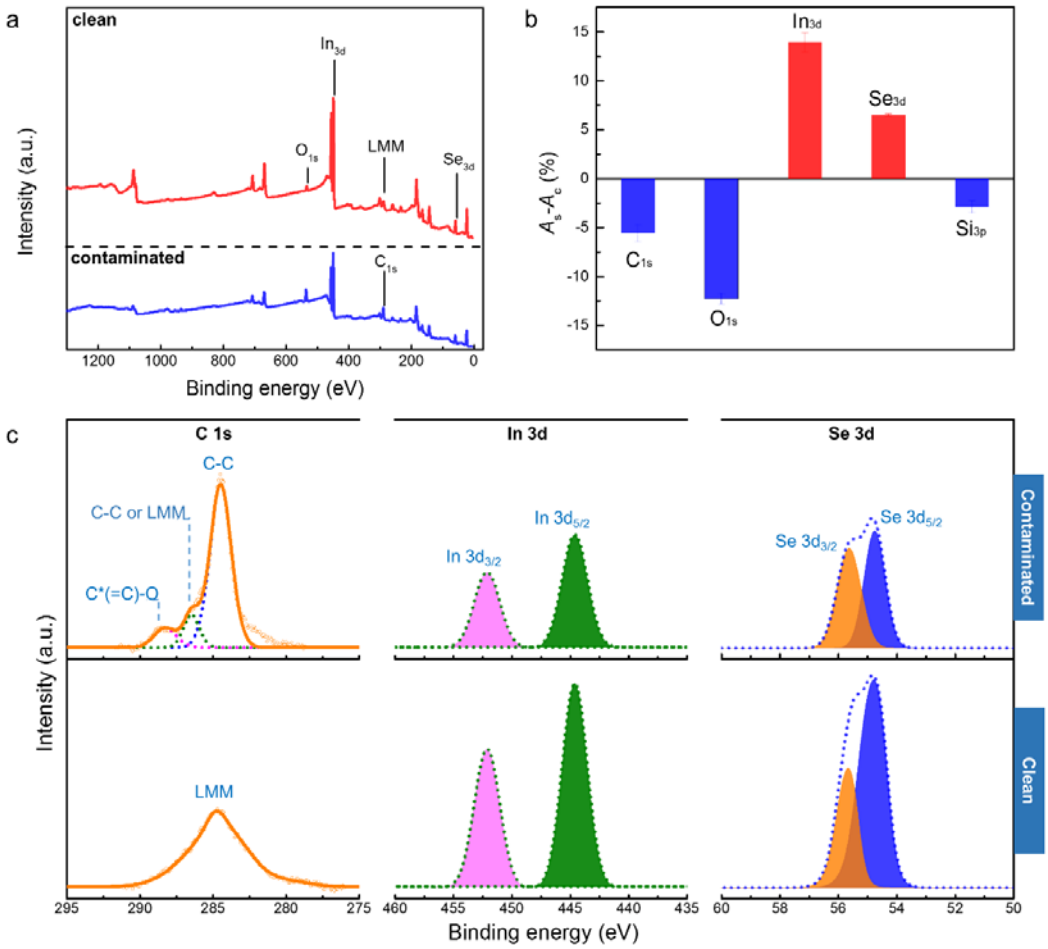

Figure 4 | Quantification of the occurrence and enrichment of carbon on InSe films. (a) Integrated compositional survey spectra from XPS for InSe films before and after surface cleaning. **(b)** Elemental atomic concentrations variation of the compositions on the InSe film before and after sputtering. **(c)** From left to right, high-resolution XPS scans of the background-subtracted and curve-fit core-level C_{1s}, In_{3d}, and Se_{3d} from InSe film before and after sputtering on the InSe film grown on SiO_2/Si. In C_{1s} core level, the peak at 285.0 eV, 286.5 eV, and 289.0 eV assigned to the C-C, C-O and the oxidized carbon, the LMM is subjected to Se auger resulted from Al Kα X-ray source. In the In_{3d} core level, the $In_{3d\,(3/2)}$ and $In_{3d\,(5/2)}$ peak at 444.6 eV and 452.2 eV were detected. In the Se_{3d} core level, $Se_{3d\,(3/2)}$ and $Se_{3d\,(5/2)}$ were at 55.7 eV and 54.8 eV, respectively.

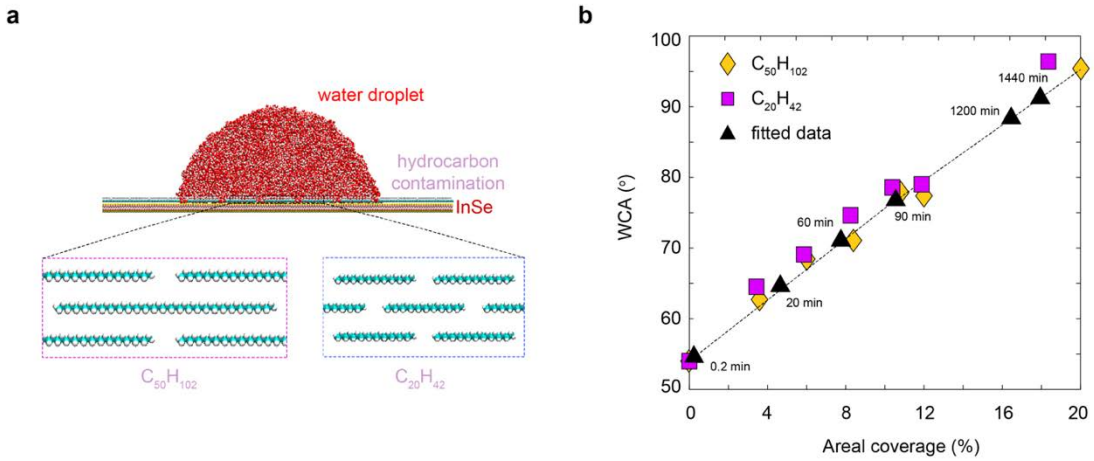

Figure 5 | MD simulations of WCAs on an InSe monolayer. (a) MD model of water droplet on the surface of monolayer InSe covered with distributed alkane chains of various length and areal coverage. **(b)** Evolution of the WCAs as a function of the areal coverage of *n*-alkane chains. The black triangles are the experimental data, where the areal coverage is extracted using the Wenzel model (see Methods for details of MD simulation setup).